Anelastic Earth structure from the coherency of the ambient seismic field

G. A. Prieto,[1] J. F. Lawrence,[2] and G. C. Beroza[2]

[1] Cross correlation of the ambient seismic field is now routinely used to measure seismic wave travel times; however, relatively little attention has been paid to other information that could be extracted from these signals. In this paper we demonstrate the relationship between the spatial coherency of the ambient field and the elastodynamic Green's function in both time and frequency domains. Through measurement of the frequency domain coherency as a function of distance, we sequentially recover phase velocities and attenuation coefficients. From these measurements we generate 1-D shear wave velocity and attenuation models for southern California. The ambient field measurements of attenuation and the exceptional path coverage that results from the many possible interstation measurements allow us to extend Q estimates over a range of frequencies that has previously been difficult to analyze using earthquake data. Measurements from paths that cross major sedimentary basins show both lower wave speeds and lower-quality factors than other paths, as expected. Our results indicate that there is a wealth of information available in the spatial coherency of the ambient seismic field.

1. Introduction

[2] It has long been known that under certain conditions it is possible to study Earth structure using the ambient seismic field. *Aki* [1957] suggested that the spatial correlation of ground motion yielded a Bessel function, which could be used to study the phase velocity beneath a seismic array. *Claerbout* [1968] conjectured that the impulse response itself could be retrieved from the temporal average of the spatial correlation. Recently, these concepts have been used by a number of investigators to generate high-resolution surface wave tomography maps for the Earth [*Shapiro et al.*, 2005; *Sabra et al.*, 2005a; *Yao et al.*, 2006; *Villaseñor et al.*, 2007; *Zheng et al.*, 2008].

[3] Surface wave tomography using earthquake records has been widely used at both global and regional scales [*Mitchell*, 1995; *Durek and Ekström*, 1996; *Romanowicz*, 2002]. This approach is limited by the uneven distribution of sources that may affect the end result. In addition, in areas with few earthquakes, tomographic studies have to rely on teleseismic earthquake sources, making it very difficult to retrieve reliable short-period measurements; however, this short-period signal is critical for constraining the structure of the crust and upper mantle.

[4] Using the ambient seismic field provides several distinct advantages for tomographic studies. First, since no earthquake sources are needed, the resolution depends mainly on station density. Second, the ambient field provides information in the period range (<20 s); whereas, in the case of earthquakes, that range is often unavailable because of attenuation. Many earthquake studies concentrate on longer periods [*Yang and Forsyth*, 2008], though results have been presented at shorter periods as well (see review by *Mitchell* [1995]).

[5] A lossless medium is assumed in many theoretical derivations of the retrieval of the Green's function from cross correlation [*Weaver and Lobkis*, 2004; *Sabra et al.*, 2005b; *Sánchez-Sesma and Campillo*, 2006]. In practice, experiments are always performed in the presence of attenuation, so in this study we examine the effects of attenuation. To first order, the coherent propagating seismic waves must have sufficient amplitude to be recorded on both receivers in order for a Green's function to be obtained, regardless of the amount of time used to calculate the correlations. Further work has shown that as long as the attenuation is small [*Roux et al.*, 2005b; *Nakahara*, 2006a; *Snieder*, 2007; *Gouédard et al.*, 2008; *Colin de Verdière*, 2009] the Green's function can be retrieved. *Roux et al.* [2005a] suggested that the attenuation may act as a low-pass filter.

[6] Attenuation will act primarily to influence ground motion amplitude. Less attention has been paid to the information carried by the amplitude of the ambient noise Green's functions. In the first experiments [*Weaver and Lobkis*, 2001] both phase and amplitude were recovered.

---

[1]Departamento de Física, Universidad de los Andes, Bogotá, Colombia.
[2]Department of Geophysics, Stanford University, Stanford, California, USA.

More recently *Larose et al.* [2007] observed that the amplitude decay agrees with the amplitude dependence expected from geometrical spreading and attenuation. *Snieder and Safak* [2006] and *Kohler et al.* [2007] showed it was possible to retrieve attenuation information for buildings using deconvolution, and *Prieto and Beroza* [2008] showed that relative amplitudes from ambient noise Green's functions obtained in this way closely matched those observed from nearby earthquakes. Some issues remain concerning whether some of the processing steps used in standard noise correlation studies [*Bensen et al.*, 2007], like prewhitening or one-bit normalization, should be employed if amplitude information is to be interpreted.

[7] Understanding the attenuation structure of the Earth is fundamental to seismology. Anelastic attenuation affects both the amplitude and phase of seismic data (because of associated dispersion). One way to study the anelastic structure of the crust and upper mantle using earthquakes is to observe the decay of surface wave amplitudes compared with the decay predicted by geometrical spreading in a purely elastic medium [*Mitchell*, 1995]. The additional decay may be due to intrinsic or scattering attenuation [*Spetzler et al.*, 2002]; however, there are other factors affecting amplitude, such as focusing and defocusing due to velocity variations and unmodeled source effects [*Dalton and Ekström*, 2006a], and these have the potential to obscure the effects of attenuation.

[8] In this study we explore the information carried by the coherency of the ambient seismic field, including its amplitude, with a focus on measuring Rayleigh wave attenuation in the crust and upper mantle. Source excitation and focusing of seismic waves by velocity structure have strong effects on wave amplitudes that can obscure the effects of attenuation. Ambient field measurements offer a particular advantage over earthquake data in this regard because of the great multiplicity of interstation paths. Because focusing should be as prevalent as defocusing, the dense path coverage and the diversity of azimuths available will tend to average out the effects of focusing.

[9] First, we briefly explain the relation between the frequency domain coherency of the ambient field and the Green's function, which links studies of the spatial autocorrelation (SPAC) and noise correlations. We then discuss our sequential phase velocity and attenuation analysis and apply it to estimate a 1-D shear wave and attenuation model for southern California. Finally, we demonstrate that paths crossing major sedimentary basins in Southern California have substantially lower wave speeds and stronger attenuation than other paths.

2. Coherency and Green's Functions

[10] If seismic surface waves are incident from all directions at equal amplitude, meaning the field is diffuse or equipartitioned, *Aki* [1957] showed that the spatial correlation of the ground motions at two stations A and B separated by a distance r, takes the form of a Bessel function

$$\langle u_A(\omega)u_B^*(\omega)\rangle = |F(\omega)|^2 J_0(kr), \tag{1}$$

where $u_A(\omega)$ and $u_B(\omega)$ are the recorded ground motion at stations A and B at angular frequency ω, k is the wave number,

$|F(\omega)|^2$ is the average spectral density of the field, the brackets $\langle\cdot\rangle$ represent the ensemble average, and the asterisk represents complex conjugate. This is the basis of the SPAC method. *Claerbout* [1968] suggested that this idea could be extended to very long distances and that the impulse response of the medium could be retrieved from the spatial correlations.

[11] It is known [*Morse and Ingard*, 1968; *Sánchez-Sesma and Campillo*, 2006] that for Rayleigh waves the Green's function in the frequency domain has the form

$$G_{AB}(\omega) = -\frac{1}{4}\mu[Y_0(kr) + iJ_0(kr)], \tag{2}$$

where Y_0 is the Neumann function (Y_0 and J_0 are Hilbert transform pairs) and thus, under equipartitioned conditions

$$\langle u_A(\omega)u_B^*(\omega)\rangle \propto Im[G_{AB}(\omega)], \tag{3}$$

where *Im* denotes the imaginary part of the function. This basic proportionality still holds if inclusions are present [*Sánchez-Sesma et al.*, 2006].

[12] The term in the brackets $\langle\cdot\rangle$, in equation (3) is called the cross spectrum. In practice, since the ambient field power $|F(\omega)|$ is nonwhite, a normalization is usually performed

$$\gamma_{AB}(\omega) = \left\langle \frac{u_A(\omega)u_B^*(\omega)}{\langle|u_A(\omega)|\rangle\langle|u_B(\omega)|\rangle} \right\rangle \propto G_{AB}(\omega), \tag{4}$$

which is called the complex coherency. It should be noted that in most studies the signals are prewhitened prior to cross correlation [*Bensen et al.*, 2007], which is equivalent to the coherency measurement proposed here.

[13] *Yokoi and Margaryan* [2008] studied the consistency of the SPAC method (using the coherency) and time domain correlations (seismic interferometry) to retrieve the Green's function and showed that (for vertical components of motion)

$$Re[\gamma_{AB}] = J_0(kr), \tag{5}$$

which shows that the coherency is proportional to the Green's function.

[14] If the ambient field is uniform, the imaginary part of the coherency $Im[\gamma_{AB}]$ will be zero, since the Fourier transform of a symmetric function is real [*Cox*, 1973]. With azimuthal averaging or enough temporal averaging this can also be achieved [*Asten*, 2006]. What these studies suggest is that the Green's function can be studied in the time domain (by Fourier transformation of the coherency) or in the frequency domain (by looking at the shape of the Bessel functions). Appendix A shows the consistency between time and frequency domains.

[15] If the medium is heterogeneous, *Honga et al.* [2005] showed that the scattering slightly changes the shape of the Bessel function. This effect is observed by *Sánchez-Sesma et al.* [2006, Figure 2] where because of a buried inclusion, the frequency domain Green's function has additional features beyond that expected for a simple J_0 shape. In the time domain, this will be represented by an additional
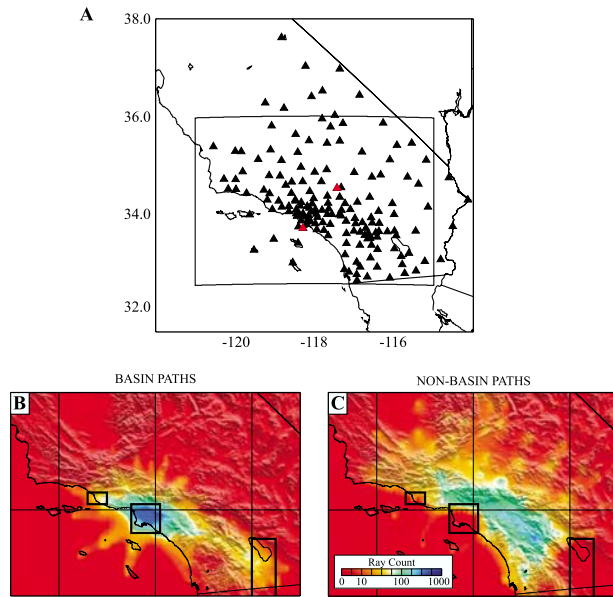
Figure 1. Area of study. (a) Map of California with seismic stations (triangles) used in this study. Boxed region shows the location of Figures 1b and 1c showing the path counts (up to 150 km long) for basin and nonbasin bins overlain on topography in the area of study. (b) Paths that have more sensitivity to major sedimentary basins, including the Ventura and Los Angeles basins and the Salton Trough, are compared to Figure 1c. (c) Paths that have less sensitivity to the basins based on their source-receiver paths. The two red triangles in Figure 1a are the stations used to calculate the coherency shown in Figure A1.

arrival. In sections 4 and 5 we investigate the frequency domain coherency and the expected effects of attenuation.

3. Data and Signal Processing

[16] We use continuous records of 154 broadband seismic stations in southern California including TriNet, Anza and USArray networks. We collected data for the entire year of 2007 for all three components, although we will focus on the vertical. Figure 1 shows the locations of the seismic stations in southern California. We also compare two distinct regions, one comprising major sedimentary basins and the other its complement.

[17] The complex-valued coherency is defined in equation (4). As it stands, this definition is unsuitable for our purposes for several reasons.

[18] 1. The recorded ambient field signals are nonstationary [Bensen et al., 2007] and include local and teleseismic earthquake signals, which contaminate the coherency estimates. In most previous studies one-bit normalization [Campillo and Paul, 2003; Bensen et al., 2007] or clipping [Sabra et al., 2005a] has been applied to the time series records before calculating the correlations or coherencies. In this study we choose to use a nonoverlapping moving window coherency estimate by taking 2-h-long segments and calculating the coherency from the raw data.

[19] 2. To add stability to equation (4) we average the denominator, i.e., the individual amplitude spectra, using a multitaper algorithm [Prieto et al., 2009] with a time-bandwidth product $NW = 3.0$ and use $K = 5$ tapers. This corresponds to a smoothing bandwidth of 0.83 mHz. Additional smoothing of the amplitude spectra in the denominator is achieved via a moving window of 20 frequency samples, corresponding to a total smoothing bandwidth of 4.4 mHz.

[20] 3. The effect of instrument glitches or pronounced earthquake signals is removed by removing 2-h-long segments that have a maximum amplitude over 100 times the RMS amplitude of the 24 h window around each segment.

[21] We start by calculating the coherency $\gamma_{AB}^{(t)}$ between a pair of seismic stations A and B for each 2 h segment using a multitaper method [Vernon et al., 1991; Park and Levin, 2000; Ma et al., 2008] where the frequency dependence is implicit. The superscript (t) represents the fact that this is an estimate for a particular 2 h window at time t. If a 2-h segment has a significant teleseismic earthquake or a spike, the coherency is not estimated.

[22] We then calculate a 1-month and 3-month coherency by averaging the multiple 2-h-long segment estimates $\gamma_{AB} = ave\{\gamma_{AB}^{(t)}\}$, where we use all $\gamma_{AB}^{(t)}$ windows fitting the criteria described above. In this paper we do not use the arithmetic mean, since the coherency does not have a Gaussian distribution [Thomson and Chave, 1991; Nolte et al., 2004]. Instead, we transform the coherency using the Z transform,

$$\tilde{\gamma}_{AB} = \frac{\gamma_{AB}}{|\gamma_{AB}|}\mathrm{atanh}(|\gamma_{AB}|), \qquad (6)$$

which has been suggested to provide a more normally distributed parameter [Thomson, 2007]. The arithmetic mean of this transformed variable is then calculated and transformed back to the original domain. We end up with 12 1-month coherencies (January, February, etc.) and 4 3-month coherencies (January–March, April–June, etc.). In Appendix A we discuss the relation between the coherency estimated here and the time domain Green's function.

[23] Given that we have around 150 stations, we can analyze more than 11,175 pairs. Thus, we only store 2,000 s of the Green's function estimate and resample the real and imaginary parts of the coherency using a 1/12 octave scale (40 samples per decade).

[24] Previous studies [Sabra et al., 2005a; Nakahara, 2006b; Asten, 2006; Yokoi and Margaryan, 2008] have asserted that either azimuthal averaging or averaging over random sources is necessary to obtain a reliable Green's function. In practice, Aki [1957] and Claerbout [1968] suggested that temporal averaging might be used instead.

[25] In order to follow the conditions more closely, we binned the coherencies $\gamma_{AB}(f)$ as a function of station separation using 1-km bins, averaging the coherency over all interstation azimuths [Vernon et al., 1991; Hough and Field, 1996; Chávez-García and Rodriguez, 2007]. This is in addition to the temporal averaging already obtained by monthly estimates. Applying this binning reduces the dimension of our data set to about 600 1-km distance bins. As shown in Figure 2 the method employed here reduces the
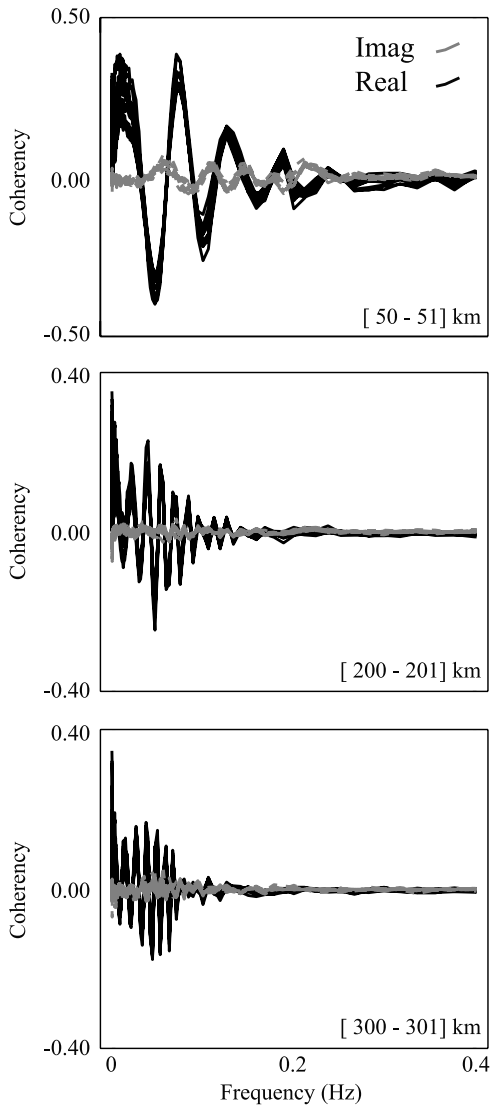
Figure 2. Twelve distinct monthly estimates of the real and imaginary parts of the coherency for three different distance bins. For higher frequencies the maximum distance at which any signal is resolved decreases, a quantity which is sometimes referred to as the decoherence length or correlation length [*Borcea et al.*, 2006; *Braun and Schweitzer*, 2008].

scatter in the data and as has been suggested [*Asten*, 2006; *Roberts and Asten*, 2008; *Yokoi and Margaryan*, 2008] the imaginary part of the coherency is significantly reduced because of the symmetry achieved.

[26] At higher frequencies (>0.25 Hz or <4 s) both the real and imaginary signal is not observed for almost all distances. This is expected given the band-limited frequency content of the microseismic noise [*Stehly et al.*, 2006].

4. Phase Velocity

[27] Following the theory developed by *Aki* [1957] and further discussed by *Asten* [2006], we use the real part of the coherency to invert for a 1-D phase velocity dispersion

curve. The coherency is related to the Bessel function of zero order by

$$\mathrm{Re}[\gamma(f,r)] = J_0\left(\frac{2\pi fr}{C(f)}\right) = J_0(kr), \qquad (7)$$

where $\gamma(f, r)$ is the average coherency for station separation r, J_0 is the zero order Bessel function for frequency f at distance r, k is wave number, and $C(f)$ is the phase velocity. We define the residual as

$$\varepsilon(f) = \mathrm{Re}[\gamma(f,r)] - J_0\left(\frac{2\pi fr}{C(f)}\right) \qquad (8)$$

and use a grid search over phase velocity from 2.0 to 6.0 km/s to find the minimum L1 residual (step size 0.005 km/s).

[28] Figure 3 shows a number of observed and predicted coherencies and the associated phase velocity estimates at various periods. The averaging of all coherencies at a given separation r is equivalent to an azimuthal average and in many cases significantly reduces the amplitudes of the imaginary part of the coherency.

[29] The monthly stacks shown in Figure 3 may be biased because of nonrandom source excitation. To test for this, we independently estimated phase velocities using the method described above for each of the 12 months of 2007. Additionally, we performed the fits on 3-month stacks instead of 1-month stacks to test whether the amount of time averaging significantly alters the results. Figure 4 shows the individual estimates obtained for 1-month and 3-month stacks. There does not seem to be any temporal dependence in the individual estimates. Also, by using more data (3 months) the average result does not change.

[30] From the phase velocities obtained above, we predict the coherency expected at each frequency and distance in the network. Figure 5 shows the observed and predicted frequency and distance-dependent coherencies using the dispersion curves obtained. At larger distances and higher frequencies the predicted coherencies have larger amplitudes than the observed. Up to now we have assumed a lossless medium, but the real Earth is anelastic and surface waves attenuate [e.g., *Spetzler et al.*, 2002; *Romanowicz*, 2002; *Yang and Forsyth*, 2008], which needs to be taken into account.

[31] The phase velocities we obtain agree with previous studies [e.g., *Yang and Forsyth*, 2006] between 25 s and 100 s period. Note that our results at longer periods are unreliable at very long wavelengths because the first zero crossing of the Bessel function is larger than the aperture of the array. At periods shorter than 5 s the amplitude of the ambient field is very small, making it difficult for coherency to persist beyond a few tens of kilometers. We have thus both insufficient signal strength and number of stations to extend the measurements to shorter periods.

5. Attenuation Coefficients

[32] Surface wave attenuation is often described by the parameter $e^{-\alpha r}$, where α is called the attenuation coefficient and is related to the surface wave quality factor Q as $\alpha = \pi f/UQ$,
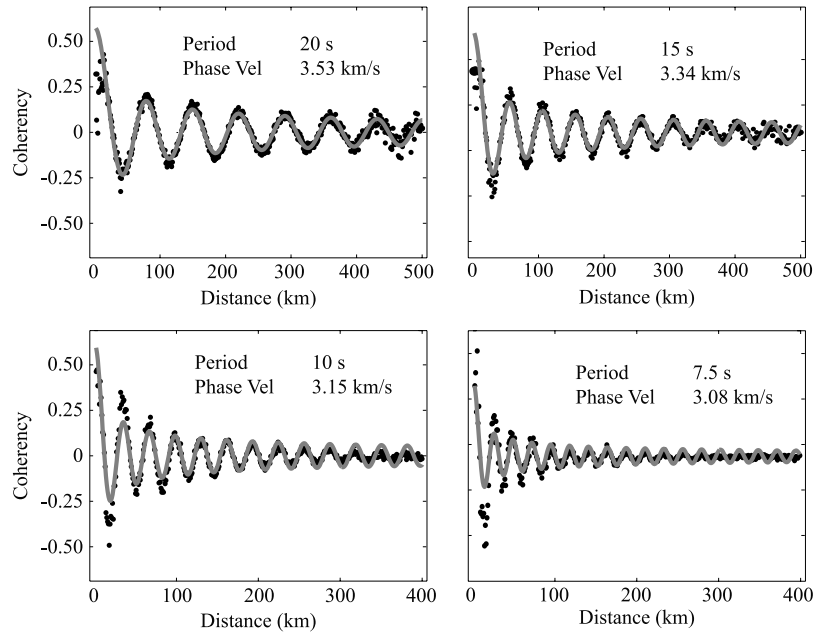
Figure 3. Observed (black dots) and predicted (gray line) coherency at different periods with minimum residual for the month of January 2007. Each plot has a description of the estimated velocity and the corresponding period.

where U is the group velocity [*Mitchell*, 1995; *Romanowicz*, 2002]. As discussed by *Weaver and Lobkis* [2006] the average of field-to-field correlations (or in our case of the coherency) is a Bessel function of order zero that is attenuated by multiple scattering and intrinsic attenuation.

[33] We modify equation (7) to take attenuation into account:

$$\mathrm{Re}[\gamma(f,r)] = J_0\left(\frac{2\pi fr}{C(f)}\right) \cdot e^{-\alpha(f)r}, \qquad (9)$$
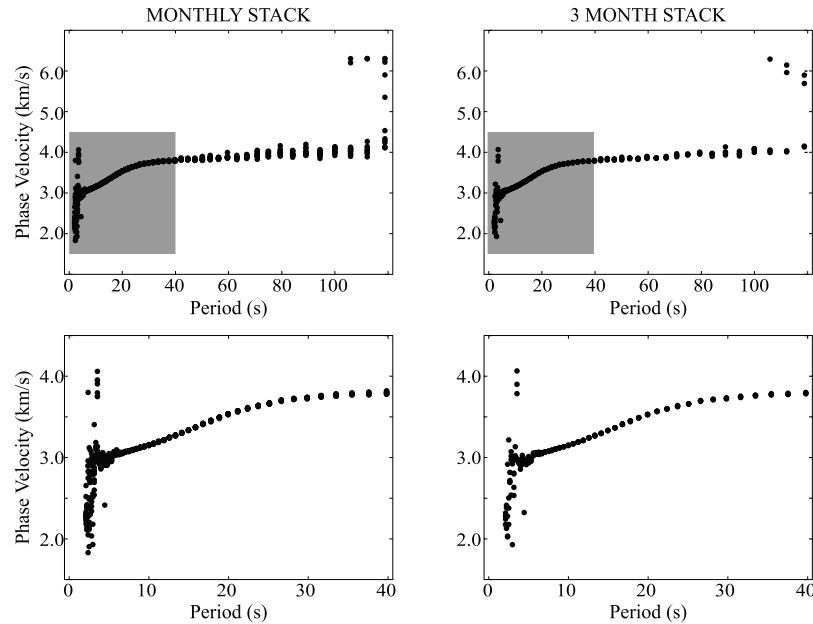
Figure 4. Phase velocity dispersion as estimated from (left) 1-month and (right) 3-month stacks of the coherency. (bottom) A zoomed version of the gray boxes above in the 0–40 s period band. For each period there are 12 1-month stack estimates and 4 3-month stacks. The spread suggests either uncertainties or some kind of temporal bias. Such a temporal bias is not observed. The 3-month stacks have smaller scatter, and their mean is similar to that obtained using 1-month stacks. Below about the 5 s period the method is no longer reliable.
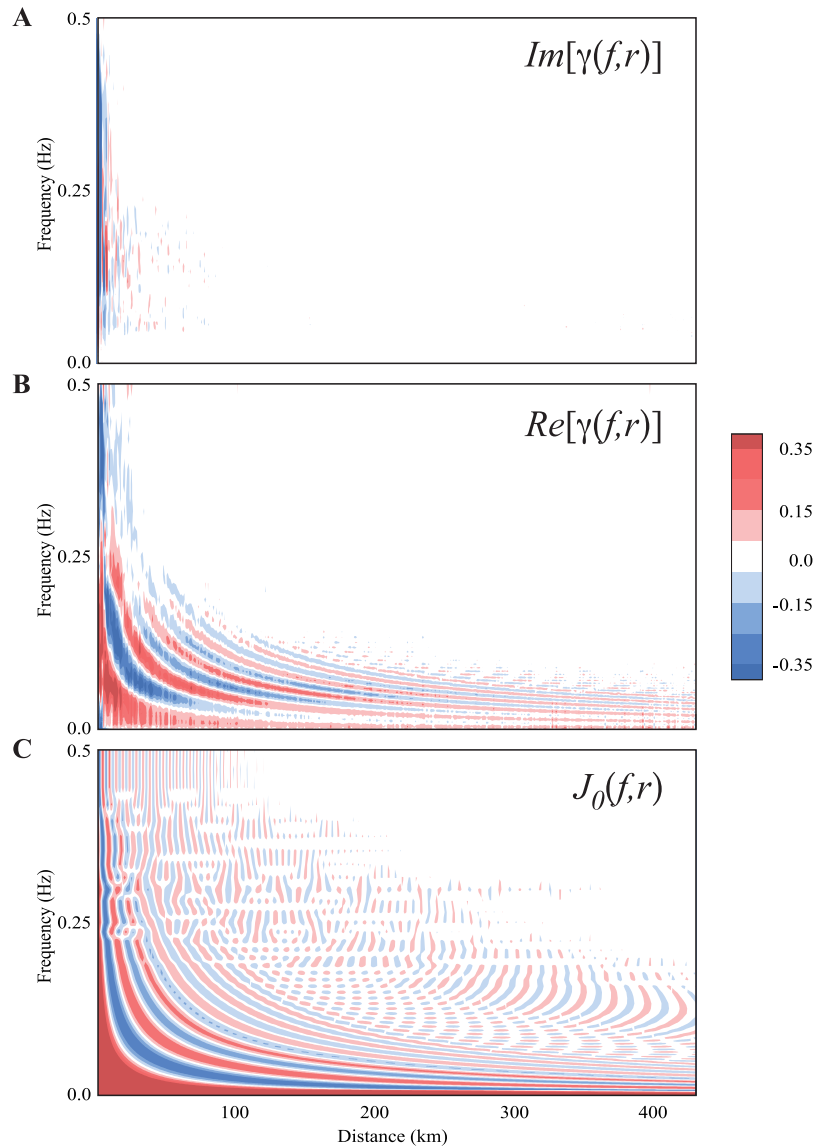
Figure 5. (a) Imaginary and (b) real observed and (c) predicted coherency by using the phase velocity dispersion shown in Figure 4. The observed imaginary and real parts of the coherency are obtained as an average over 3 months. Note that at large distances or higher frequencies the predicted signal continues ringing, while the observed data merges into the background noise. We suggest the observed excess damping is due to attenuation. Note that the amplitude of the imaginary component is small over most distances and frequencies.

where α is the frequency-dependent attenuation coefficient. As equation (9) suggests, coherency decreases more rapidly in the presence of anelasticity or multiple scattering. We use the observed excess decay relative to the elastic case to find the attenuation coefficient as a function of frequency. For example, in Figure 3 the observed coherency has peaks and troughs up to a certain distance, after which the observed signals behave randomly. The theoretical model predicts continuing wiggles, which are not present in the data. We tested different binning criteria (0.1–10 km) with similar results, showing that this effect is not due to the averaging used.

[34] In order to model the attenuation coefficient we calculate the logarithm of the envelope of both the theoretical and data coherency as a function of distance, using our previous estimate of the velocity $C(f)$. The envelopes are smoothed over half a wavelength (smoothing is frequency- and velocity-dependent), and a measure of the standard deviation of the data is taken for each distance. We perform a second grid search to find the minimum L1 misfit, for reasonable values of the attenuation coefficient $\alpha(f)$. Figure 6 shows an example of the fit between the theoretical model and the observed coherency for various periods.

[35] We investigate the uncertainty in the attenuation coefficient estimates and whether bias is introduced by temporal changes in the noise sources or by the amount of data used in computing the coherencies (1- versus 3-month stacks). Figure 3 shows that the velocity estimation is not reliable at short periods (<5 s), so we limit our attenuation estimates to the period band 5–40 s. At longer
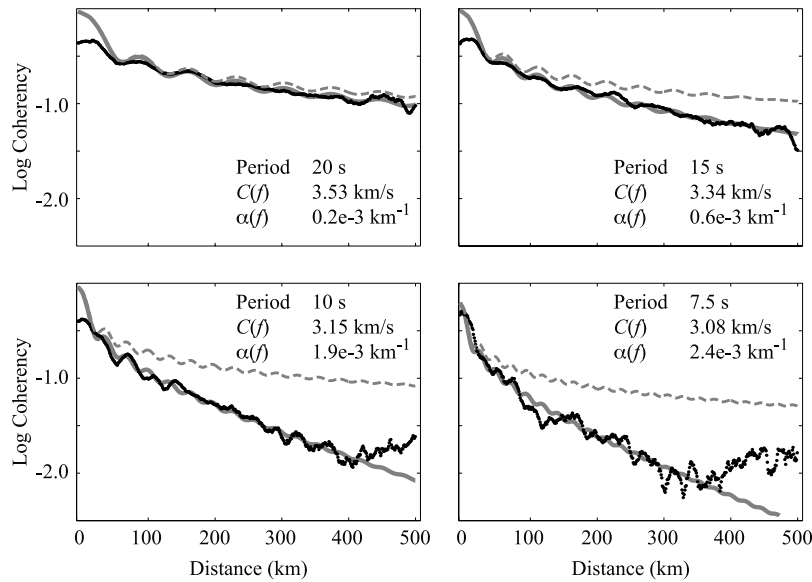
Figure 6. Observed (black dots) and best fit coherency without attenuation correction (gray dashed line) and with attenuation (gray solid line) for the month of January 2007 at four periods. A value of log amplitude of −2.0 is used as a threshold where given 1 month of data the coherency at greater distances is not significant. Each plot has a description of the estimated velocity and attenuation coefficient and the corresponding period.

periods (>40 s) we have good velocity estimates, but the waves propagate only a few wavelengths and thus the amplitudes do not decay enough for a reliable attenuation measurement.

[36] In this study we focus on the attenuation coefficients in the period band between 5 and 20 s, which can be difficult to study using surface waves from earthquakes because of the combination of strong attenuation and high microseismic noise. To our knowledge there have been no surface wave attenuation studies in southern California in this period range. *Yang and Forsyth* [2008] studied the attenuation coefficient for 25 s periods and longer and *Mitchell* [1995] compiled a number of 5−20 s studies in Asia, the Basin and Range, and elsewhere.
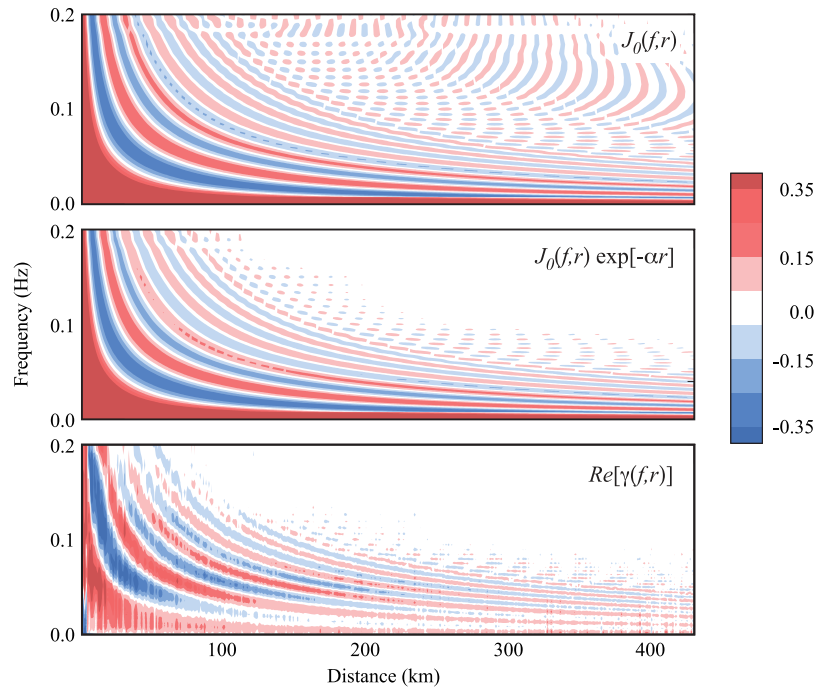
[37] The values of the attenuation coefficients (see Figure 7) range from $(0.27 \pm 0.1) \times 10^{-3}$ km^{-1} at 20 s to $(2.7 \pm 0.3) \times 10^{-3}$ km^{-1} at 7.5 s, and $(6.4 \pm 1.3) \times 10^{-3}$ km^{-1} at 5 s period. These results are higher than the compiled studies presented by *Mitchell* [1995], but are similar to results for the Tibetan Plateau [*Jemberie and Mitchell*, 2004, 2005] where a more attenuating crust is expected. The combination of high temperature and active tectonics might explain the strong attenuation we observe [*Olsen et al.*, 2003; *Erickson et al.*, 2004; *Hauksson and Shearer*, 2006]. Figure 8 shows the observed and predicted coherencies (compare to Figure 5) with and without the attenuation coefficients obtained above.

6. One-Dimensional Phase and Q Model Inversion

[38] From the results obtained in sections 4 and 5 we solve for 1-D velocity and Q as a function of depth beneath southern California. For details on the inversion method we refer the reader to [*Mokhtar et al.*, 1988; *Mitchell*, 1995;
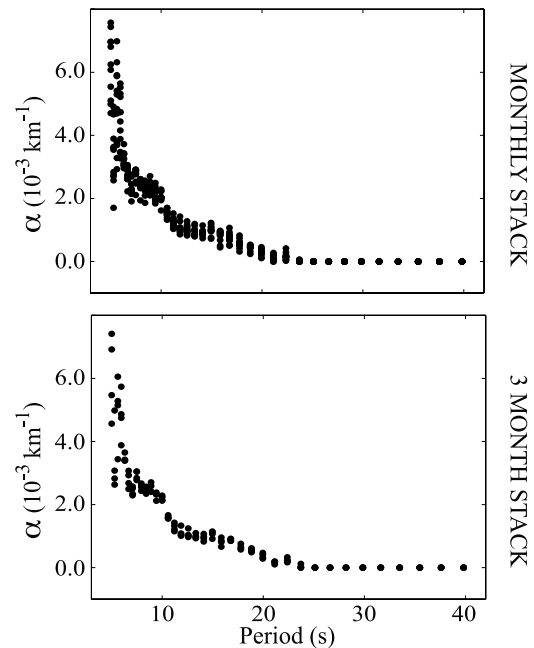
Figure 7. Attenuation coefficient as a function of period as estimated from (top) 1-month and (bottom) 3-month stacks of the coherency, similar to Figure 4. The scatter suggests the uncertainties become significant below the 7 s period. No temporal bias is observed. The 3-month stacks have smaller scatter, and their mean is similar to that obtained using 1-month stacks. At longer periods (>20 s) the amplitude decay is small such that our method is unable to extract an accurate estimate of $\alpha(f)$. *Yang and Forsyth* [2008] suggest a value of about 0.26 10^{-3} at 25 s, which is similar to the value we obtain at 20 s.

Figure 8. Predicted coherency from phase velocity estimates (top) without and (middle) with attenuation corrections. (bottom) The observed coherencies are better described with the attenuation coefficients used in modeling. The observed real part of the coherency is obtained as an average over 3 months. Note that compared to Figure 5 the amplitudes at larger distances and higher frequencies are correctly predicted.

Shapiro and Ritzwoller, 2002; *Romanowicz*, 2002; *Herrmann and Ammon*, 2004; *Yang and Forsyth*, 2006]. The relation between surface wave dispersion and the shear wave velocity with depth is nonlinear. We use the iterative linearized inversion developed by *Herrmann and Ammon* [2004] to solve for velocity (and later Q) for a number of layers as a function of depth.

[39] The attenuation coefficient at a given period, T, can be represented as a sum of shear wave quality factors (Q_μ^{-1}) in each layer of the model once a velocity structure is estimated. The attenuation follows

$$\alpha(T) = \frac{\pi}{C_R^2 T} \sum_{i=1}^{N} \left[\left(\beta_i \frac{\partial C_R}{\partial \beta_i} \right) + \frac{1}{2} \left(\alpha_i \frac{\partial C_R}{\partial \alpha_i} \right) \right] Q_{\mu_i}^{-1}, \qquad (10)$$

where the subscript R denotes Rayleigh waves, α_i, β_i are the P and S wave velocities at layer i, C_R is the phase velocity obtained from the dispersion curves, and the partial derivatives include the effects of the sensitivity of each period with depth as well as the effect of layer thickness.

[40] We assume a constant velocity, constant Q_μ starting model, and parameterize the model using 45 layers spanning 0 to 150 km depth. The layer thickness is 2 km for the upper 50 km and 5 km below. We use phase velocity measurements from the ambient noise analysis spanning 5 to 85 s. This allows us to resolve V_S to ~100 km depth. Our measurements of the attenuation coefficient are limited to 5–20 s because of the limited aperture of the network as described previously. This would limit our resolution of Q_μ to ~40 km depth; however, we supplement our observations

with measurements from *Yang and Forsyth* [2008] so that we can resolve Q_μ to 100 km depth as well.

[41] Figure 9 shows the phase velocity and attenuation coefficient estimates and the associated V_S and Q_μ models obtained in one inversion. The velocity model is similar to the one obtained by *Yang and Forsyth* [2006] in southern California, and correctly predicts the observations.

[42] *Mitchell* [1995] observed that Q_μ rapidly increases with depth in the upper crust and starts decreasing with depth in the lower crust. The transition between increasing and decreasing Q_μ varies depending on the tectonic setting of the region studied. *Al-Khatib and Mitchell* [1991] found that in the eastern US the transition likely occurs in the 30–50 km depth range, while in the Basin and Range it occurs in the 20–30 km depth range [*Mitchell and Xie*, 1994]. *Yang and Forsyth* [2008] suggest the transition occurs somewhat deeper, however their model is poorly resolved in the upper 50 km. Our period range for the Q_μ models is most sensitive to the upper 40 km, and the combined data can better constrain this transitional depth. The resultant model is shown in Figure 9d, and shows the transition starting at about 30 km depth.

[43] The values we obtain for Q_μ in our results are physically realistic. For the shallowest layers the values of Q_μ range from about 40 to 60, which agrees with previous results in California [*Al-Khatib and Mitchell*, 1991; *Abercrombie*, 1997; *Olsen et al.*, 2003] and is slightly lower than obtained in the Basin and Range [*Patton and Taylor*, 1984; *Mitchell and Xie*, 1994; *Mitchell*, 1995].

[44] Using borehole records *Abercrombie* [1997, 1998] suggested a low $Q < 100$ value for the upper 3 km of the
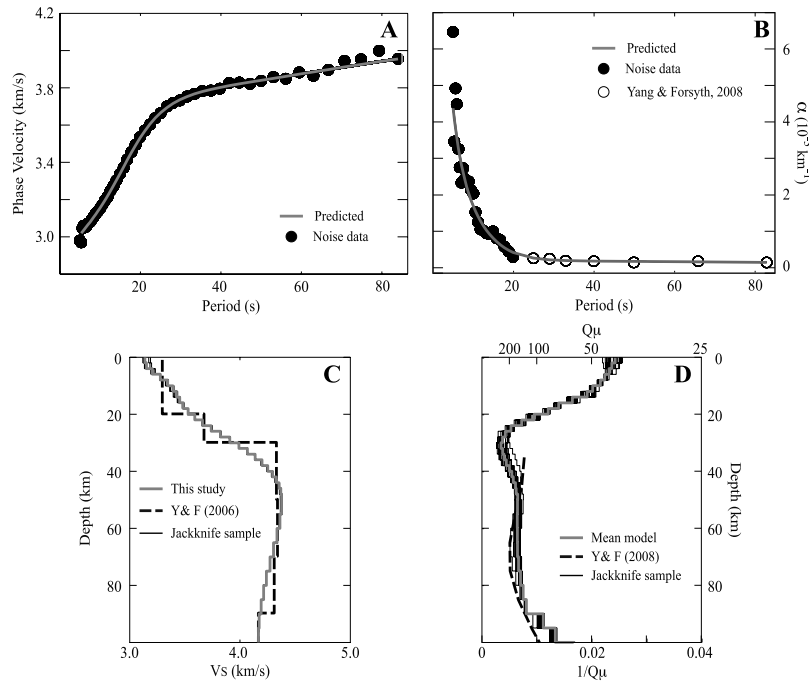
Figure 9. Shear wave velocity V_S and Q_μ models for our study region. The observed and the predicted (a) phase velocities and (b) attenuation coefficients for the mean model. For the attenuation coefficient we used additional data [*Yang and Forsyth*, 2008] for periods longer than 20 s. (c and d) Various models are obtained by using a jackknife resampling [*Prieto et al.*, 2007] of the phase and attenuation data between 5 and 20 s. In each turn one sample is removed before estimating the model. The V_S and Q_μ models of *Yang and Forsyth* [2006, 2008] are shown for reference. A rapid decrease in Q_μ (larger attenuation) in the shallower crust is observed. The spread of the different jackknifed models can be thought of as a way of investigating the bounds and resolution at each depth.

crust in agreement with more recent results [*Schlotterbeck and Abers*, 2001; *Olsen et al.*, 2003]. Depth-dependent attenuation models obtained using spectral amplitudes from *P* and *S* waves [*Schlotterbeck and Abers*, 2001; *Hauksson and Shearer*, 2006] show a rapid increase of *Q* with depth shallower than ∼5 km depth. Our results have very low Q_μ values in the shallow layers that agree with these studies; however Q_μ increases more gradually to a lower maximum Q_μ value at 30 km depth.

[45] This discrepancy could result from one or more of several underlying causes. First, the slow increase in our Q_μ model with depth could be due to smoothing of the models in our inversions. We tested a suite of damping parameters, however, and obtained either very similar results or unreasonable variability between adjacent layers, suggesting that our result is robust.

[46] A second possibility is that the attenuation coefficients we obtained include scattering attenuation in addition to intrinsic attenuation [*Brandenburg and Snieder*, 1989; *Romanowicz*, 2002; *Spetzler et al.*, 2002], while direct *P* and *S* waves are affected less by scattering. The effects of scattering in the coherency are indistinguishable from that of intrinsic attenuation as we processed the data [*Weaver and Lobkis*, 2006; *Campillo*, 2006]. Nevertheless, because scattering should be strongest at shallow depths within the basin, and those results agree between the studies, scattering is not likely the cause of the discrepancy.

[47] Third, discrepancies could arise because of source effects or multipathing in the earthquake-based studies, which should effect ambient noise studies less because of receiver-receiver path symmetry. Finally, intrinsic attenuation is frequency-dependent, which can cause Q_μ to increase from 200 for a 7-s Rayleigh wave to >600 for a 10 Hz *P* or *S* wave given a frequency dependence of $Q = Q_0 f^{[0.25 - 0.5]}$ [e.g., *Raoof et al.*, 1999; *Rietbrock*, 2001; *Erickson et al.*, 2004].

7. Attenuation in Major Sedimentary Basins

[48] So far we have examined the possibility of using noise to gather information about average phase velocity and seismic attenuation using an entire regional array (southern California) as an example. An important question is whether this method can provide information on more localized properties, for example velocity and attenuation in the basins compared to other regions. Following *Patton and Taylor* [1984], we regionalized our analysis to compare basin and nonbasin paths.

[49] From the available data in southern California we selected raypaths that have sensitivity to the major basins, including the Los Angeles Basin, the Ventura Basin and the Salton Trough. We then compare both the coherency and log coherency of these raypaths to all other paths, i.e., those that are not directly crossing those same basins (see maps in Figure 1).
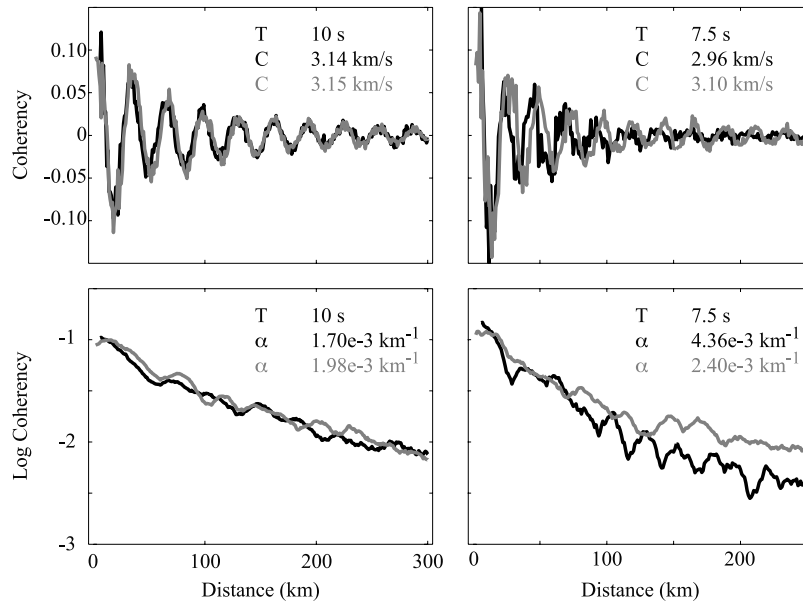
Figure 10. Coherency of raypaths in major southern California basins versus other raypaths. (top) The real part of the coherency for basin paths (black) versus the nonbasin paths (gray), showing a significant difference in phase velocities at the 7.5 s period. (bottom) In terms of amplitude decay the basin paths are more attenuating, and the coherency decays more quickly. Each plot shows the estimated phase velocity and attenuation coefficient obtained for the 3-month stack.

[50] Figure 10 shows the real parts of the coherency for basin and nonbasin paths in southern California at two selected frequencies as a function of station separation. At 10 s period both signals align and decay similarly with distance. At shorter periods (7.5 s) significant differences emerge. The coherency for the basin paths indicates a lower phase velocity compared to nonbasin paths (closer spacing of the zero crossings in the Bessel function). In addition, the log coherency decays more quickly for basin paths, suggesting a larger attenuation coefficient, by a factor of ~2, at shorter periods.
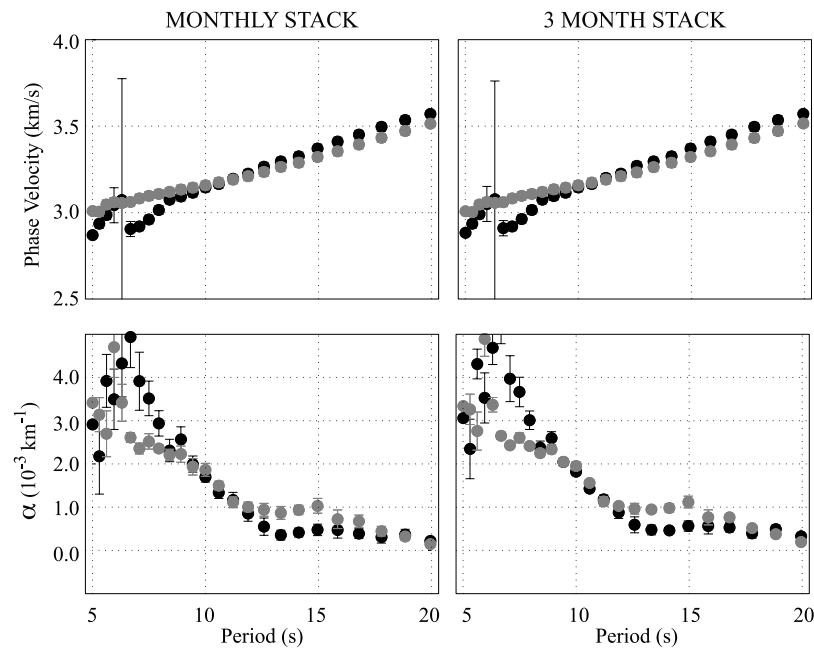
Figure 11. Phase velocity and attenuation coefficients for basin (black) versus nonbasin (gray) paths. Note that for longer periods both phase velocity and attenuation coefficients are similar for the two regions, but in the 7–10 s period the basin paths are lower and attenuate surface waves more for the basins.

[51] We estimate phase velocity and attenuation coefficients (see Figure 11) for each of the 12 monthly subsets of the coherency estimates. When we subdivide the data set like this, we inevitably have fewer raypaths to average over, resulting in larger uncertainties. In the 7–15 s period range, the phase velocity estimates have very similar values, but start to diverge for the shorter periods (see for example Figure 11). In particular between 7 and 10 s the basin path phase velocities are significantly lower, as expected [*Magistrale et al.*, 2000; *Shapiro et al.*, 2005; *Sabra et al.*, 2005a].

[52] The attenuation coefficient also shows clearly distinct behavior for the two regions. The basin paths have a larger attenuation coefficient (by as much as a factor of two (Figure 10)) at shorter periods. These shorter periods have sensitivities concentrated in the shallow crust, reflecting the influence of the slower and more attenuative sedimentary deposits in these major basin [*Olsen et al.*, 2003; *Hauksson and Shearer*, 2006].

8. Discussion and Conclusions

[53] Our results show that the spatial coherency of the ambient seismic field provides a great deal of information about elastic and anelastic Earth structure. The methodology we apply differs from previous studies of noise correlations in that we do not apply any temporal normalization [see, e.g., *Bensen et al.*, 2007]. Sign bit normalization potentially suppresses information on the relative amplitude of the reconstructed signals between the components [*Larose*, 2006; *Larose et al.*, 2007]; however, preliminary results [*Matzel*, 2007] suggest that even sign bit signals may preserve amplitude information. In this paper we use the coherency of the ambient field to show how attenuation can be recovered, which demonstrates that spectral whitening can indeed preserve amplitude information.

[54] The results we obtain are consistent with, and complement, results obtained using earthquake data at longer periods. Our data provides high-resolution estimates for periods shorter than 20 s, thus being mostly sensitive to the upper 40 km. The depth dependence of the Q_μ model we obtain may be attributable to the presence of fluids in the crust especially in sedimentary basins. The fractured crust in southern California may also contribute to the low overall Q_μ compared to nontectonic regions such as the eastern US [*Mitchell*, 1995].

[55] The separation of intrinsic and scattering attenuation has received significant attention in the past [*Aki*, 1980; *Richards and Menke*, 1983; *Wu*, 1985; *Sato and Fehler*, 1998; *Lacombe et al.*, 2003]. The attenuation coefficient obtained here may include both the effects of intrinsic and scattering attenuation. We have not attempted to differentiate between them and we caution the reader that scattering may produce similar effects on the coherency. Without increased resolution, differentiation between these contributing factors is not possible. If one-bit signals have meaningful amplitude information, it may suggest attenuation due to scattering, since it is the multiply scattered waves that are being amplified [*Campillo and Paul*, 2003] and the coherency will decrease with increasing scattering.

[56] There are other strong effects on the amplitudes of surface waves that have the potential to undermine attempts to measure attenuation. These include the source of the ambient field and the focusing effects of complex velocity structure [*Dalton and Ekström*, 2006a, 2006b]. For the latter case, ambient field measurements offer a particular advantage over earthquake data. Over all possible paths, focusing is as prevalent as defocusing, and the multitude of station-to-station paths combined with the ambient noise approach ensure extensive azimuthal averaging. The binning of coherency as a function of distance should effectively suppress the focusing effect of velocity structure on amplitude.

[57] We have also investigated possible effects of a time-varying source excitation of the ambient field, but our examination of individual monthly stacks show no evidence for significant bias introduced by source variability. We argue this is likely because of the extensive temporal and azimuthal averaging intrinsic to our approach.

[58] We have shown that this method can be adapted for regionalized comparisons [e.g., *Patton and Taylor*, 1984] of distinct regions or structural features, demonstrating how the attenuation coefficient and velocity structure varies with location. We compared interstation paths that are strongly sensitive to major sedimentary basins with paths with little sensitivity and find that sedimentary basins in southern California are characterized by low velocity and stronger attenuation, as expected [*Olsen et al.*, 2003]. Further work will investigate to what extent this method can lead to localize velocity and attenuation anomalies.

[59] We have shown how both phase velocities and attenuation coefficients can be retrieved from the spatial coherency. A similar relation exists for Love waves [*Yokoi and Margaryan*, 2008], although more complicated than for Rayleigh waves. Incorporating phase velocity and attenuation coefficients for Love waves and using all 3 components of motion is an obvious future research direction.
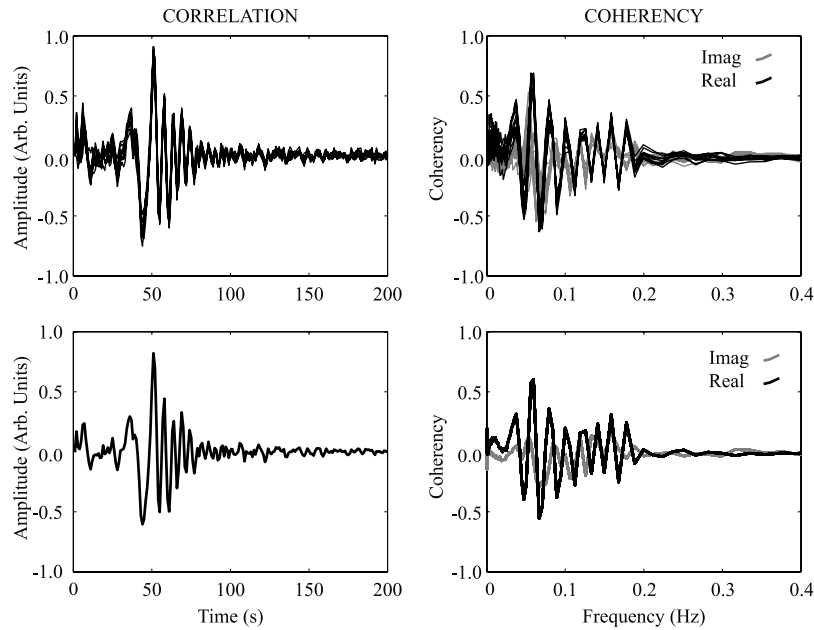
Appendix A: Relation Between Time and Frequency Domains

[60] Many studies [*Chávez-García and Luzón*, 2005; *Sánchez-Sesma and Campillo*, 2006; *Nakahara*, 2006a; *Chávez-García and Rodriguez*, 2007; *Yokoi and Margaryan*, 2008] propose a relation between the time domain spatial correlations (cross correlations) and the frequency domain correlations (SPAC method, or spatial coherency). In this section we corroborate this relationship with our very complete data set.

[61] As explained by *Sánchez-Sesma and Campillo* [2006] the relation arises from the fact that the imaginary part of the frequency domain Green's function for Rayleigh waves has the shape of a Bessel function in a homogeneous medium. *Yokoi and Margaryan* [2008] also demonstrated this relation in a more practical approach (note however that the definition of coherency used in that article is not the standard one).

[62] From the average coherency γ_{AB} we retrieve the time domain Green's function estimate by inverse Fourier transformation

$$\hat{G}_{AB}(t) = \mathcal{F}^{-1}[\gamma_{AB}(f)], \qquad (A1)$$

Figure A1. Time and frequency information extracted from the ambient field between two stations ADO and FMP. (top) Individual results for 1-month stacks and (bottom) the average of all monthly stacks. (left) The time domain correlations (showing 200 s) is expected to converge to the impulse response between the seismic stations as if there were a virtual source at station ADO recorded at station FMP. The frequency domain can be modeled by a Bessel function of order zero. The coherency is calculated from the two stations marked as red triangles in Figure 1.

where $\mathcal{F}^{-1}$ represents inverse Fourier transformation and $\hat{G}_{AB}$ is the estimated Green's function as obtained by correlation of the ambient field. Note that equation (A1) is equivalent to a time domain correlation after each signal has been prewhitened [*Bensen et al.*, 2007]. Figure A1 shows the relation between the frequency and time domain descriptions of the coherency/correlation for stations ADO and FMP for 12 single-month stacks.

[63] Here we show that this relation extends to at least regional distances. We generate a set of synthetic Green's functions for a selected set of distances and inverse Fourier transform

$$G(t, r) = \mathcal{F}^{-1}\{[Y_0(kr) + iJ_0(kr)]e^{-\alpha r}\}, \qquad (A2)$$

where $k = 2\pi f/C$, and the frequency-dependent phase velocity (C) and attenuation coefficient (α) were obtained in sections 4 and 5, respectively. As pointed out by *Sánchez-Sesma and Campillo* [2006] from J_0 we can calculate Y_0 and all the information regarding the Green's function can be constructed.

[64] Figure A2 shows the predicted and observed Green's functions at two distinct frequency bands, obtained by binning all data as a function of interstation distance, as we did for the coherency. The observed and predicted Green's functions are very similar. In agreement with *Harmon et al.* [2008] we apply a $\pi/4$ for comparing the theoretical and observed Green's functions.

[65] We obtained phase velocity estimate from the time domain Green's functions [see, e.g., *Yao et al.*, 2006] similar to the results obtained in section 4. Figure A3 shows the record section of the time domain Green functions for the

entire network. The phase velocities obtained from the coherency fits, agree with the time domain observations.

[66] Note that in the 10–20 s period range the phase velocity is easily distinguishable from the group velocity. At
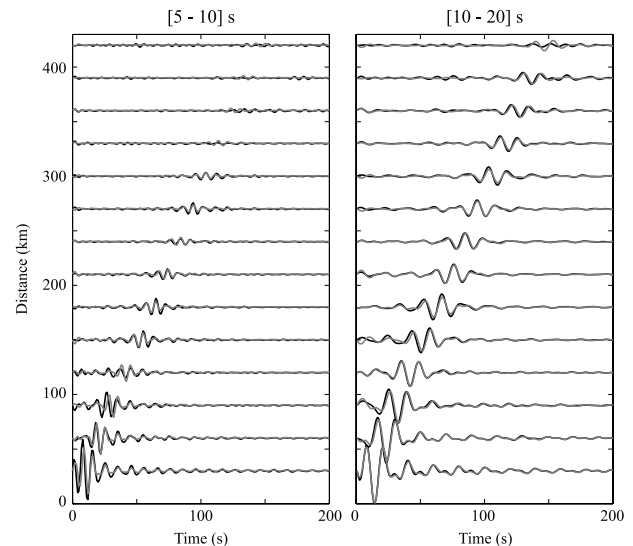
Figure A2. Consistency of the time and frequency domain descriptions of the Green's functions for two frequency bands, (left) 5–10 s and (right) 10–20 s. Selected distance bins of the observed Green's functions from the ambient seismic field (black) and the predicted ones using the phase velocity and attenuation coefficients obtained previously. Note that both the observed and theoretical Green's functions have decreasing amplitude with distance.
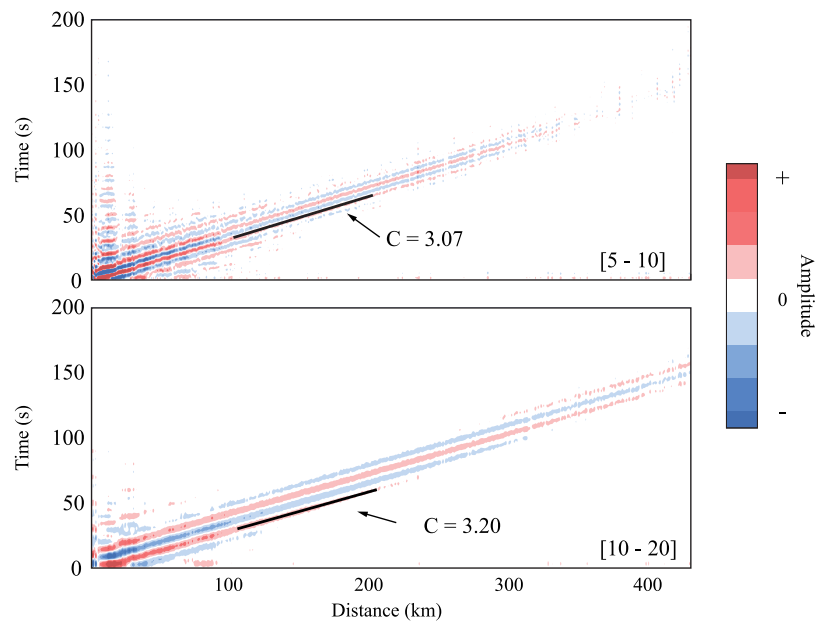
Figure A3. Record section of the time domain Green's functions obtained in southern California in two distinct frequency bands. In each plot the black line represents the predicted phase delay calculated from the average estimate in the appropriate frequency bands from Figure 4.

higher frequencies the phase and group velocities are close together, which again is in agreement with the observations. The group velocity is related to the phase velocity [*Aki and Richards*, 1980] by $U = C + k \, dC/d\omega$. In Figure 4 we observe that the slope of the phase velocity ($dC/d\omega$) is smaller for the shorter periods, thus the group velocity U is similar to the phase velocity C in that frequency range.

References

Abercrombie, R. E. (1997), Near-surface attenuation and site effects from comparison of surface and deep borehole recordings, *Bull. Seismol. Soc. Am.*, *87*(3), 731–744.

Abercrombie, R. E. (1998), A summary of attenuation measurements from borehole recordings of earthquakes: The 10 Hz transition problem, *Pure Appl. Geophys.*, *153*, 475–487.

Aki, K. (1957), Space and time spectra of stationary stochastic waves, with special reference to microtremors, *Bull. Earthquake Res. Inst. Univ. Tokyo*, *35*, 415–457.

Aki, K. (1980), Scattering and attenuation of shear waves in the lithosphere, *J. Geophys. Res.*, *85*, 6496–6504.

Aki, K., and P. Richards (1980), *Quantitative Seismology*, W. H. Freeman, New York.

Al-Khatib, H. H., and B. J. Mitchell (1991), Upper mantle anelasticity and tectonic evolution of the western United States from surface wave attenuation, *J. Geophys. Res.*, *96*, 18,129–18,146.

Asten, M. W. (2006), On bias and noise in passive seismic data from finite circular array data processed using SPAC methods, *Geophysics*, *71*(6), V153–V162.

Bensen, G. D., M. H. Ritzwoller, M. P. Barmin, A. L. Levshin, F. Lin, M. P. Moschetti, N. M. Shapiro, and Y. Yang (2007), Processing seismic ambient noise data to obtain reliable broad-band surface wave dispersion measurements, *Geophys. J. Int.*, *169*, 1239–1260, doi:10.1111/j.1365-246X.2007.03374.x.

Borcea, L., G. Papanicolaou, and C. Tsogka (2006), Coherent interferometric imaging in clutter, *Geophysics*, *71*(4), SI165–SI175.

Brandenburg, A., and R. Snieder (1989), The attenuation of surface waves due to scattering, *Geophys. J. Int.*, *98*, 183–194.

Braun, T., and J. Schweitzer (2008), Spatial noise-field characteristics of a three-component small aperture test array in central Italy, *Bull. Seismol. Soc. Am.*, *98*(4), 1876–1886.

Campillo, M. (2006), Phase and correlation in "random" seismic fields and the reconstruction of the Green function, *Pure Appl. Geophys.*, *163*, 475–502, doi:10.1007/s00024-005-0032-8.

Campillo, M., and A. Paul (2003), Long-range correlations in the diffuse seismic coda, *Science*, *299*, 547–549.

Chávez-García, F. J., and F. Luzón (2005), On the correlation of seismic microtremors, *J. Geophys. Res.*, *110*, B11313, doi:10.1029/2005JB003671.

Chávez-García, F. J., and M. Rodriguez (2007), The correlation of microtremors: Empirical limits and relations between results in frequency and time domains, *Geophys. J. Int.*, *171*, 657–664, doi:10.1111/j.1365-246X.2007.03529.x.

Claerbout, J. F. (1968), Synthesis of a layered medium from its acoustic transmission response, *Geophysics*, *33*(2), 264–269.

Colin de Verdière, Y. (2009), Semiclassical analysis and passive imaging, *Nonlinearity*, *22*, R45–R75, doi:10.1088/0951-7715/22/6/R01.

Cox, H. (1973), Spatial correlation in arbitrary noise fields with application to ambient sea noise, *J. Acoust. Soc. Am.*, *54*(5), 1289–1301.

Dalton, C. A., and G. Ekström (2006a), Global models of surface wave attenuation, *J. Geophys. Res.*, *111*, B05317, doi:10.1029/2005JB003997.

Dalton, C. A., and G. Ekström (2006b), Constraints on global maps of phase velocity from surface-wave amplitudes, *Geophys. J. Int.*, *167*, 820–826, doi:10.1111/j.1365-246X.2006.03142.x.

Durek, J. J., and G. Ekström (1996), A radial model of anelasticity with long-period surface wave attenuation, *Bull. Seismol. Soc. Am.*, *86*(1A), 144–158.

Erickson, D., D. E. McNamara, and H. M. Benz (2004), Frequency-dependent Lg Q within the continental United States, *Bull. Seismol. Soc. Am.*, *94*(5), 1630–1643.

Gouédard, P., et al. (2008), Cross-correlation of random fields: Mathematical approach and applications, *Geophys. Prospect.*, *56*, 375–393.

Harmon, N., P. Gerstoft, C. A. Rychert, G. A. Abers, M. Salas de la Cruz, and K. M. Fischer (2008), Phase velocities from seismic noise using beamforming and cross correlation in Costa Rica and Nicaragua, *Geophys. Res. Lett.*, *35*, L19303, doi:10.1029/2008GL035387.

Hauksson, E., and P. M. Shearer (2006), Attenuation models (Q_P and Q_S) in three dimensions of the southern California crust: Inferred fluid saturation at seismogenic depths, *J. Geophys. Res.*, *111*, B05302, doi:10.1029/2005JB003947.

Herrmann, R. B., and C. J. Ammon (2004), *Computer Programs in Seismology: Surface Waves, Receiver Functions and Crustal Structure*, Saint Louis Univ., St. Louis, Mo.

Honga, T.-K., R.-S. Wu, and B. L. N. Kenneth (2005), Stochastic features of scattering, *Phys. Earth Planet. Inter.*, 148, 131–148.

Hough, S. E., and E. H. Field (1996), On the coherence of ground motion in the San Fernando Valley, *Bull. Seismol. Soc. Am.*, 86(6), 1724–1736.

Jemberie, A. L., and B. J. Mitchell (2004), Shear-wave Q structure and its lateral variation in the crust of China and surrounding regions, *Geophys. J. Int.*, 157, 363–380.

Jemberie, A. L., and B. J. Mitchell (2005), Frequency-dependent shear-wave Q models for the crust of China and surrounding regions, *Pure Appl. Geophys.*, 162, 21–36.

Kohler, M. D., T. H. Heaton, and S. C. Bradford (2007), Propagating waves in the steel, moment-frame factor building recorded during earthquakes, *Bull. Seismol. Soc. Am.*, 97(4), 1334–1345.

Lacombe, C., M. Campillo, A. Paul, and L. Margerin (2003), Separation of intrinsic absorption and scattering attenuation from Lg coda decay in central France using acoustic radiative transfer theory, *Geophys. J. Int.*, 154, 417–425.

Larose, E. (2006), Mesoscopics of ultrasound and seismic waves: Application to passive imaging, *Ann. Phys. Fr.*, 31(3), 1–126.

Larose, E., P. Roux, and M. Campillo (2007), Reconstruction of Rayleigh-Lamb dispersion spectrum based on noise obtained from an air-jet forcing, *J. Acoust. Soc. Am.*, 122(6), 3437–3444.

Ma, S., G. A. Prieto, and G. C. Beroza (2008), Testing community velocity models for southern California using the ambient seismic field, *Bull. Seismol. Soc. Am.*, 98(6), 2694–2714, doi:10.1785/0120080947.

Magistrale, H., S. Day, R. W. Clayton, and R. Graves (2000), The SCEC southern California reference three-dimensional seismic velocity model version 2, *Bull. Seismol. Soc. Am.*, 90(6B), S65–S76.

Matzel, E. (2007), Imaging seismic attenuation in the crust and upper mantle by ambient noise correlation, *Eos Trans. AGU*, 88(52), Fall Meet. Suppl., Abstract S33E-08.

Mitchell, B. J. (1995), Anelastic structure and evolution of the continental crust and upper mantle from seismic surface wave attenuation, *Rev. Geophys.*, 33(4), 441–462.

Mitchell, B. J., and J. Xie (1994), Attenuation of multiphase surface waves in the Basin and Range Province—III. Inversion for crustal anelasticity, *Geophys. J. Int.*, 116, 468–484.

Mokhtar, T. A., R. B. Herrmann, and D. R. Russell (1988), Seismic velocity and Q model for the shallow structure of the Arabian shield from short-period Rayleigh waves, *Geophysics*, 53(11), 1379–1387.

Morse, P. M., and K. U. Ingard (1968), *Theoretical Acoustics*, McGraw-Hill, New York.

Nakahara, H. (2006a), Theoretical background of retrieving Green's function by cross-correlation: One-dimensional case, *Geophys. J. Int.*, 165, 719–728.

Nakahara, H. (2006b), A systematic study of theoretical relations between spatial correlation and Green's function in one-, two- and three-dimensional random scalar wavefields, *Geophys. J. Int.*, 167, 1097–1105.

Nolte, G., O. Bai, L. Wheaton, Z. Mari, S. Vorbach, and M. Hallett (2004), Identifying true brain interaction from EEG data using the imaginary part of coherency, *Clin. Neurophysiol.*, 115, 2292–2307.

Olsen, K. B., S. M. Day, and C. R. Bradley (2003), Estimation of Q for long-period (>2 sec) waves in the Los Angeles Basin, *Bull. Seismol. Soc. Am.*, 93(2), 627–638.

Park, J., and V. Levin (2000), Receiver functions from multiple-taper spectral correlation estimates, *Bull. Seismol. Soc. Am.*, 90(6), 1507–1520.

Patton, H. J., and S. R. Taylor (1984), Q structure of the Basin and Range from surface waves, *J. Geophys. Res.*, 89, 6929–6940.

Prieto, G. A., and G. C. Beroza (2008), Earthquake ground motion prediction using the ambient seismic field, *Geophys. Res. Lett.*, 35, L14304, doi:10.1029/2008GL034428.

Prieto, G. A., D. J. Thomson, F. L. Vernon, P. M. Shearer, and R. L. Parker (2007), Confidence intervals for earthquake source parameters, *Geophys. J. Int.*, 168, 1227–1234, doi:10.1111/j.1365-246X.2006.03257.x.

Prieto, G. A., R. L. Parker, and F. L. Vernon (2009), A Fortran 90 library for multitaper spectrum analysis, *Comput. Geosci.*, doi:10.1016/j.cageo.2008.06.007, in press.

Raoof, M., R. B. Herrmann, and L. Malagnini (1999), Attenuation and excitation of three-component ground motion in southern California, *Bull. Seismol. Soc. Am.*, 89(4), 888–902.

Richards, P. G., and W. Menke (1983), The apparent attenuation of a scattering medium, *Bull. Seismol. Soc. Am.*, 73(4), 1005–1021.

Rietbrock, A. (2001), P wave attenuation structure in the fault area of the 1995 Kobe earthquake, *J. Geophys. Res.*, 106, 4141–4154.

Roberts, J., and M. Asten (2008), A study of near source effects in array-based (SPAC) microtremor surveys, *Geophys. J. Int.*, 174, 159–177.

Romanowicz, B. (2002), Inversion of surface waves: A review, in *International Handbook of Earthquake and Engineering Seismology Part A*, edited by W. Lee, pp. 149–173, Academic, Amsterdam.

Roux, P., K. G. Sabra, P. Gerstoft, W. A. Kuperman, and M. C. Fehler (2005a), P-waves from cross-correlation of seismic noise, *Geophys. Res. Lett.*, 32, L19303, doi:10.1029/2005GL023803.

Roux, P., K. G. Sabra, W. A. Kupperman, and A. Roux (2005b), Ambient noise cross correlation in free space: Theoretical approach, *J. Acoust. Soc. Am.*, 117(1), 79–84.

Sabra, K. G., P. Gerstoft, P. Roux, W. A. Kuperman, and M. C. Fehler (2005a), Surface wave tomography from microseisms in southern California, *Geophys. Res. Lett.*, 32, L14311, doi:10.1029/2005GL023155.

Sabra, K. G., P. Roux, and W. A. Kuperman (2005b), Emergence rate of the time-domain Green's function from the ambient noise cross-correlation function, *J. Acoust. Soc. Am.*, 118(6), 3524–3531.

Sánchez-Sesma, F. J., and M. Campillo (2006), Retrieval of the Green's function from cross correlation: The canonical elastic problem, *Bull. Seismol. Soc. Am.*, 96(3), 1182–1191, doi:10.1785/0120050181.

Sánchez-Sesma, F. J., J. A. Pérez-Ruiz, M. Campillo, and F. Luzón (2006), Elastodynamic 2D Green function retrieval from cross-correlation: Canonical inclusion problem, *Geophys. Res. Lett.*, 33, L13305, doi:10.1029/2006GL026454.

Sato, H., and M. Fehler (1998), *Seismic Wave Propagation and Scattering in the Heterogeneous Earth*, Springer, New York.

Schlotterbeck, B. A., and G. A. Abers (2001), Three-dimensional attenuation variations in southern California, *J. Geophys. Res.*, 106, 30,719–30,735.

Shapiro, N. M., and M. H. Ritzwoller (2002), Monte-Carlo inversion for a global shear-velocity model of the crust and upper mantle, *Geophys. J. Int.*, 151, 88–105.

Shapiro, N., M. Campillo, L. Stehly, and M. Ritzwoller (2005), High-resolution surface wave tomography from ambient seismic noise, *Science*, 307, 1615–1618.

Snieder, R. (2007), Extracting the Green's function of attenuating heterogeneous acoustic media from uncorrelated waves, *J. Acoust. Soc. Am.*, 121(5), 2637–2644.

Snieder, R., and E. Safak (2006), Extracting the building response using seismic interferometry: Theory and application to the Millikan Library in Pasadena, California, *Bull. Seismol. Soc. Am.*, 96(2), 586–598.

Spetzler, J., J. Trampert, and R. Snieder (2002), The effect of scattering in surface wave tomography, *Geophys. J. Int.*, 149, 755–767.

Stehly, L. M., M. Campillo, and N. M. Shapiro (2006), A study of the seismic noise from its long-range correlation properties, *J. Geophys. Res.*, 111, B10306, doi:10.1029/2005JB004237.

Thomson, D. J. (2007), Jackknifing multitaper spectrum estimates, *IEEE Signal Process. Mag.*, 24(4), 20–30.

Thomson, D. J., and A. D. Chave (1991), Jackknife error estimates for spectra, coherences, and transfer functions, in *Advances in Spectrum Analysis and Array Processing*, vol. 1, edited by S. Haykin, chap. 2, pp. 58–113, Prentice Hall, Englewood Cliffs, N. J.

Vernon, F. L., J. Fletcher, L. Haar, A. Chave, and E. Sembera (1991), Coherence of seismic body waves from local events as measured by a small aperture array, *J. Geophys. Res.*, 96, 11,981–11,996.

Villaseñor, A., Y. Yang, M. H. Ritzwoller, and J. Gallart (2007), Ambient noise surface wave tomography of the Iberian Peninsula: Implications for shallow seismic structure, *Geophys. Res. Lett.*, 34, L11304, doi:10.1029/2007GL030164.

Weaver, R. L., and O. I. Lobkis (2001), Ultrasonics without a source: Thermal fluctuation correlations at MHz frequencies, *Phys. Rev. Lett.*, 87, 134,301.

Weaver, R. L., and O. I. Lobkis (2004), Diffuse fields in open systems and the emergence of the Green's function, *J. Acoust. Soc. Am.*, 116(5), 2731–2734.

Weaver, R. L., and O. I. Lobkis (2006), Diffuse fields in ultrasonics and seismology, *Geophysics*, 71(4), S15–S19.

Wu, R.-S. (1985), Multiple scattering and energy transfer of seismic waves: Separation of scattering effect from intrinsic attenuation—I. Theoretical modelling, *Geophys. J. R. Astron. Soc.*, 82, 57–80.

Yang, Y., and D. W. Forsyth (2006), Rayleigh wave phase velocities, small-scale convection, and azimuthal anisotropy beneath southern California, *J. Geophys. Res.*, 111, B07306, doi:10.1029/2005JB004180.

Yang, Y., and D. W. Forsyth (2008), Attenuation in the upper mantle beneath southern California: Physical state of the lithosphere and asthenosphere, *J. Geophys. Res.*, 113, B03308, doi:10.1029/2007JB005118.

Yao, H., R. D. van der Hilst, and M. V. de Hoop (2006), Surface-wave array tomography in SE Tibet from ambient seismic noise and two-station analysis—I. Phase velocity maps, *Geophys. J. Int.*, 166, 732–744.

Yokoi, T., and S. Margaryan (2008), Consistency of the spatial autocorrelation method with seismic interferometry and its consequence, *Geophys. Prospect.*, 56, 435–451, doi:10.1111/j.1365-2478.2008.00709.x.

Zheng, S., X. Sun, X. Song, Y. Yang, and M. H. Ritzwoller (2008), Surface wave tomography of China from ambient seismic noise correlation, *Geochem. Geophys. Geosyst.*, *9*, Q05020, doi:10.1029/2008GC001981.

———————————

G. C. Beroza and J. F. Lawrence, Department of Geophysics, Stanford University, Stanford, CA 94305, USA.

G. A. Prieto, Departamento de Física, Universidad de los Andes, Carrera 1 No. 18A 10, Bogotá, Colombia. (gprieto@uniandes.edu.co)